



HAL
open science

The Fast Evolving, Tremendous Blue Superoutburst in ASASSN-21au Reveals a Dichotomy in the Outbursts of Long-period AM CVns

L.E. Rivera Sandoval, C.O. Heinke, J.M. Hameury, Y. Cavecchi, T. Vanmunster, T. Tordai, F.D. Romanov

► **To cite this version:**

L.E. Rivera Sandoval, C.O. Heinke, J.M. Hameury, Y. Cavecchi, T. Vanmunster, et al.. The Fast Evolving, Tremendous Blue Superoutburst in ASASSN-21au Reveals a Dichotomy in the Outbursts of Long-period AM CVns. *The Astrophysical Journal*, 2022, 926 (1), pp.10. 10.3847/1538-4357/ac3fb7 . hal-03318493

HAL Id: hal-03318493

<https://hal.science/hal-03318493v1>







Submitted on 20 Jun 2022

HAL is a multi-disciplinary open access archive for the deposit and dissemination of scientific research documents, whether they are published or not. The documents may come from teaching and research institutions in France or abroad, or from public or private research centers.

L'archive ouverte pluridisciplinaire **HAL**, est destinée au dépôt et à la diffusion de documents scientifiques de niveau recherche, publiés ou non, émanant des établissements d'enseignement et de recherche français ou étrangers, des laboratoires publics ou privés.



The Fast Evolving, Tremendous Blue Superoutburst in ASASSN-21au Reveals a Dichotomy in the Outbursts of Long-period AM CVns

L. E. Rivera Sandoval¹ , C. O. Heinke¹ , J. M. Hameury² , Y. Cavecchi³ , T. Vanmunster⁴ , T. Tordai⁵, and F. D. Romanov⁶ 

¹ University of Alberta, Department of Physics, CCIS 4-183, T6G 2E1, Edmonton, AB, Canada; liliana.riverasandoval@utrgv.edu

² Observatoire astronomique de Strasbourg, Université de Strasbourg, CNRS UMR 7550, F-67000 Strasbourg, France

³ Universidad Nacional Autónoma de México, Instituto de Astronomía, Ciudad Universitaria, CDMX 04510, Mexico

⁴ CBA Belgium Observatory & CBA Extremadura Observatory, Walhostraat 1a, B-3401 Landen, Belgium

⁵ Polaris Observatory, Hungarian Astronomical Association, Laborc u. 2/c, 1037 Budapest, Hungary

⁶ AAVSO observer, Russia

Received 2021 July 21; revised 2021 November 27; accepted 2021 December 1; published 2022 February 8

Abstract

ASASSN-21au is an ultracompact accreting white dwarf binary (AM CVn type) with a period of ~ 58 minutes. Using multiwavelength observations of the system, we discovered a dichotomy in the behavior of outbursts in AM CVns. The binary showed an initial increase in brightness that lasted for at least 82 days, followed by an additional increase that lasted two weeks. Afterward, ASASSN-21au went into superoutburst with a total duration of 19 days, showing an amplitude with respect to quiescence of ~ 7.5 mag in g , with a precursor and an echo outburst. A correlation between X-rays, UV, and optical was identified for the first time in an AM CVn during this stage. The color evolution of ASASSN-21au indicates that during the superoutburst the dominant component was the accretion disk. The short duration, large amplitude, and color evolution of the superoutburst agree with expectations from the disk instability model. These characteristics are opposite to those observed in SDSS J080710+485259 and SDSS J113732+405458, which have periods of ~ 53 minutes and ~ 60 minutes, respectively. The initially slow increase in brightness in the light curve of ASASSN-21au and the behavior after the superoutburst favor a scenario in which changes in the mass-transfer rate led to disk instabilities, while the outburst mechanism of SDSS J080710+485259 and SDSS J113732+405458 has been attributed to enhanced mass transfer alone. Further observations are needed to understand the origin of this dichotomy.

Unified Astronomy Thesaurus concepts: AM Canum Venaticorum stars (31); White dwarf stars (1799); Stellar accretion disks (1579); X-ray binary stars (1811); Cataclysmic variable stars (203); Hydrogen deficient stars (769); Interacting binary stars (801); Close binary stars (254); Compact binary stars (283)

1. Introduction

AM CVns are a relatively poorly studied class of accreting white dwarf (WD) binaries. Having typical orbital periods (P_{orb}) between 5 and 70 minutes (e.g., Ramsay et al. 2018; Green et al. 2020), AM CVns include the accreting binaries with the shortest orbits known so far, which makes them important sources of low-frequency gravitational waves that can be detected by LISA (Breivik et al. 2018; Liu et al. 2021, and references therein).

AM CVns share several similarities with the cataclysmic variables (CVs), especially dwarf novae (DNe). However, unlike CVs, where the donor is hydrogen-rich, AM CVns are hydrogen-poor. The latter can be produced through three principal channels, depending on the initial state of the donor when mass transfer starts: the donor can be a fully degenerate white dwarf, either He or C/O (e.g., Pringle & Webbink 1975; Tutukov & Yungelson 1979), a semidegenerate helium core-burning star (Savonije et al. 1986), or a subgiant (leading to the exposure of the semidegenerate hydrogen-deficient core; Tutukov et al. 1985; Nelson et al. 1986). Depending on which evolutionary channel is followed, the chemical composition of the donor will change (e.g., Nelemans et al. 2010). The orbital

periods of CVs are also much longer, with typical values of 85 minutes to 10 hr.

As occurs in the case of CVs, the evolution of AM CVns after reaching the period minimum (e.g., Iben & Tutukov 1991; Yungelson 2008) dictates that the mass-transfer rate from the companion reduces as the binary evolves. The degenerate nature of the donor star causes the binary's orbit to become wider with time (e.g., Tutukov et al. 1985). These binaries also become progressively fainter with time, which makes them difficult to detect when in quiescence. However, for the AM CVns that show a transient behavior (like DNe in regular CVs), their brightness increases by several magnitudes during DN-like outbursts, making them detectable by all-sky optical surveys (e.g., Levitan et al. 2013; van Roestel et al. 2021a). Most AM CVns known so far have been identified in this way.

According to the standard disk instability model (see review by Hameury 2020, and references therein), the presence of outbursts in AM CVns depends on the mass-transfer rate. Observationally a dividing line occurs at periods around $P_{\text{orb}} = 20$ minutes. For shorter periods, the high mass-transfer rate ensures the disks are hot and stable, hence no outbursts are expected, while at longer periods the disk builds up to intermittent outbursts. However, unlike the case of CVs, for AM CVns the mass-transfer rate at relatively long orbital periods is expected to be so low that the accretion disk becomes cold and stable again, so outbursts are not expected to be observed either. The lower limit on orbital period for that



Original content from this work may be used under the terms of the [Creative Commons Attribution 4.0 licence](https://creativecommons.org/licenses/by/4.0/). Any further distribution of this work must maintain attribution to the author(s) and the title of the work, journal citation and DOI.

phenomenon is not really clear, either theoretically (due to the several free parameters in the models) or observationally.

Further complications have recently been added by observations of long-period AM CVns in outbursts (Rivera Sandoval et al. 2020, 2021), which suggest that enhanced mass transfer also plays a very important role as an outburst-triggering mechanism.

In this paper we present multiwavelength observations of a recently discovered AM CVn star, known as ASASSN-21au, which was identified spectroscopically during outburst and which had a variable superhump period (a period in which the disk precesses, close to the orbital period; Patterson et al. 2005) between 57 and 60 minutes (Isogai et al. 2021, vsnet-alert 25369).⁷ The observations of ASASSN-21au discussed here demonstrate that there is a dichotomy in the behavior of outbursts in long-period AM CVns.

2. Observations and Data Analysis

2.1. Swift X-Ray and UV Observations

We have obtained X-ray and UV data of ASASSN-21au during its first superoutburst and post-outburst cooling phase with the XRT and UVOT instruments on board the Neil Gehrels Swift Observatory (Swift). Data were taken from 2021 February 17 to 2021 June 11 with a total exposure time of 12 ks distributed in 14 observations.

ASASSN-21au was detected in X-rays in nine of the observations, with upper limits on the remaining measurements, mainly due to the short exposure times. The XRT data analysis was performed using XSPEC (Arnaud 1996, Version 12.11). Count rates were obtained in the X-ray energy range 0.3–10 keV for each of the individual observations. For the spectral analysis we used an absorbed power-law model ($tbabs^*powerlaw$), fixing N_H to the Galactic value of $2.87 \times 10^{20} \text{ cm}^{-2}$ toward the position of the source. In order to obtain meaningful values for the spectral fits we divided the observations into two groups: those obtained during the plateau phase of the superoutburst and those taken during the post-outburst cooling phase where the binary was detected. For each group we binned the data considering at least five counts per bin and used Cash statistics (Cash 1979) due to the low number of counts acquired.

For each individual Swift observation, UVOT data were obtained in the six available filters: *UVW2*, *UVM2*, *UVW1*, *U*, *B*, and *V*, which in total cover the wavelength range from 1600 to 8000 Å. Data were analyzed with the suggested tools in the Swift threads.⁸ For the background subtraction we used a circular region of $5''$ radius around the target, and a circular region with a radius of $25''$ was used to determine the background. Photometry was calibrated to the AB system.

2.2. Optical and Additional UV Observations

Data in the clear and *V* filters were obtained by members of the AAVSO (Kafka 2021) and VSNET with the first measurement starting on 2021 February 12 and the last one taken on 2021 April 15. Several epochs with cadences of 1 minute per observation were obtained. We have aligned the data from the different observers into a common frame by using

⁷ We have chosen to use an average superhump period of 58.4 minutes as obtained from a Lomb–Scargle (Lomb 1976; Scargle 1982) analysis.

⁸ <https://www.swift.ac.uk/analysis/uvot/>

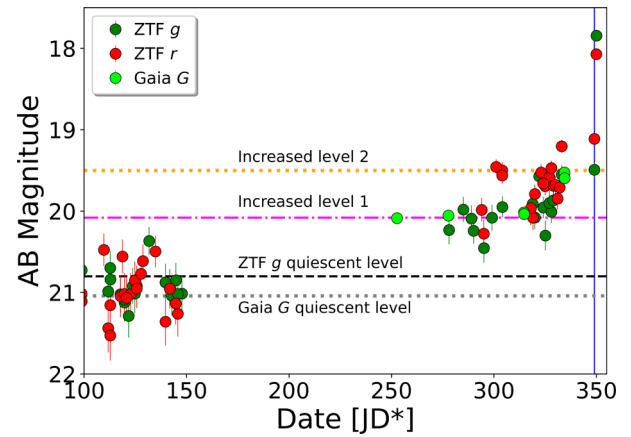


Figure 1. Optical light curve of ASASSN-21au during quiescence and the first indications of increases in brightness. The blue vertical line denotes the beginning of the precursor of the superoutburst.

the first data set of observations as reference, which is consistent with the results from the Swift *V* filter.

For comparison purposes we have also made use of public observations from the ATLAS project in the cyan and orange bands (Tonry et al. 2018) and from ZTF (Masci et al. 2019) in the *g* and *r* bands. Only data with good quality flags have been used for the analysis. Additionally, in the case of the ZTF data, we excluded points with airmass >1.8 since the differential chromatic refraction that produces color biases dominates above that value (Masci et al. 2019). We also used data from ASAS-SN (Shappee et al. 2014; Kochanek et al. 2017) in the *g* band, from Pan-STARRS (Chambers et al. 2016) in the *g*, *r*, *i*, and *z* bands, from GALEX (Bianchi et al. 2011) in the near-UV (NUV), and from Gaia EDR3 (Gaia Collaboration 2020) and the Gaia alerts⁹ in the *G* band. Photometry from these surveys is reported here in the AB system.

We also checked for indications of previous outburst activity from the binary in the ATLAS, ASAS-SN, ZTF, CSS (Drake et al. 2009), and DASCH (Grindlay et al. 2009) databases, but no outbursts of similar amplitude to the one reported here were previously recorded.

3. Results

3.1. The Multiwavelength Light Curve of ASASSN-21au

The multiwavelength light curves of ASASSN-21au are shown in Figures 1 and 2. The first increase in brightness of ASASSN-21au was detected by Gaia on 2020 October 30 ($\text{JD}^* = 252.7$, where $\text{JD}^* = \text{JD} - 2,458,900$) when the binary was 1 mag above (marked as increased level 1) its original *G* quiescence level. On 2020 November 24 ($\text{JD}^* = 278$) ZTF *g* detected the binary at the same increased level 1 (corresponding to ~ 0.8 mag above its ZTF *g* quiescent level). Constraints due to the Sun prevented a good coverage with ZTF to observe the rise phase, but based on the current ZTF and Gaia data, a limit on the duration of the rise and the increased level 1 (τ_{L1}) can be determined as $67 \text{ days} < \tau_{L1} < 172 \text{ days}$. On $\text{JD}^* = 333$ the binary reached a second increased brightness level (marked with an orange line in Figures 1 and 2), which was 1.5 mag above the original Gaia *G* quiescent value. The system took approximately two additional weeks to reach that level and remained in such a state for another two weeks. On 2021

⁹ <http://gsaweb.ast.cam.ac.uk/alerts/alert/Gaia21cbs/>

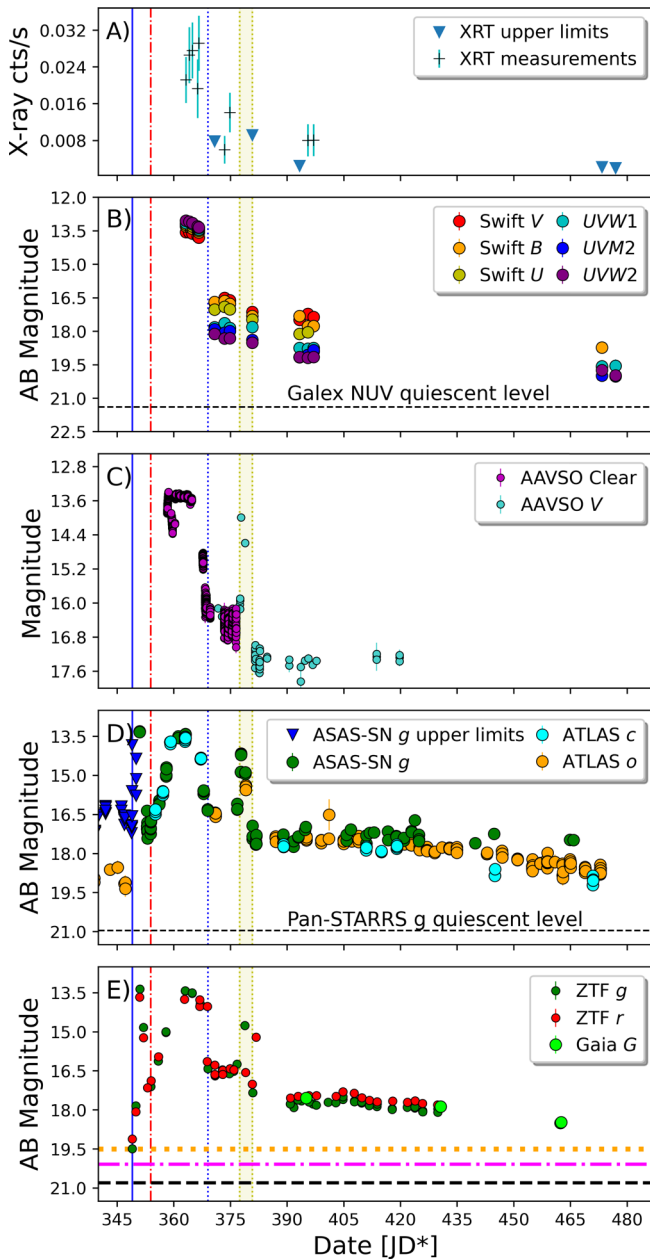


Figure 2. Multiwavelength light curve of ASASSN-21au during superoutburst. The beginning was determined using ZTF data and is marked with a blue solid line. The blue dotted line indicates the end of the superoutburst and the beginning of the post-outburst cooling phase. The dashed red line marks the end of the precursor, and the yellow band denotes the period where an echo outburst occurred between $\text{JD}^* = 378$ and 381 . (A) XRT light curve in the energy range 0.3–10 keV. X-ray detections during the post-outburst cooling phase are signatures of residual accretion. (B) Multiband UVOT observations. They are simultaneous with the X-ray data. The GALEX NUV quiescent level is indicated with a black dashed line. (C) Fast (1 minute) cadence AAVSO data. Periodic oscillations due to superhumps were detected in the superoutburst. (D) Light curves with data from the ASAS-SN and ATLAS surveys. (E) Gaia and ZTF light curves. The beginning of the precursor was detected on $\text{JD}^* = 349$. The colors of the horizontal lines have the same meaning as those in Figure 1.

February 3 ($\text{JD}^* = 349$) ASASSN-21au showed a sudden increase in brightness due to the precursor of the superoutburst (denoted with a solid blue vertical line in Figures 1 and 2).

The first ASAS-SN solid detections of ASASSN-21au were three points at $g \sim 13$ mag on 2021 February 5 ($\text{JD}^* = 351$), followed by several other points 2–3 days later at $g \sim 16.4$ – 17.4 mag, which indicate the fading of the precursor.

Afterwards the rise to the plateau phase started. The maximum of the precursor was similar to the maximum of the plateau (~ 7.5 mag in g above its ZTF quiescent level). While precursors are common in DNe of the type SU UMa and they have recently been confirmed in multiple AM CVns (Duffy et al. 2021; Pichardo Marcano et al. 2021), they are relatively difficult to detect using ground-based images due to their short duration. But continuous coverage of AM CVns’ superoutbursts with space telescopes now suggests that precursors are a relatively common characteristic (Pichardo Marcano et al. 2021). In the case of the precursor of ASASSN-21au, it is also remarkable that its luminosity drops by three magnitudes right before the superoutburst begins, much more so than in any other system (Duffy et al. 2021; Pichardo Marcano et al. 2021).

In the bluest UV band ($UVW2$), there was a decrease of three orders of magnitude in flux between the plateau of the superoutburst and the post-outburst cooling phase around $\text{JD}^* = 373.3$, going from $1.60 \times 10^{-13} \text{ erg s}^{-1} \text{ cm}^{-2}$ to $3.36 \times 10^{-16} \text{ erg s}^{-1} \text{ cm}^{-2}$, while in the V band the flux decreased by only two orders of magnitude, showing that the dominant emission components during superoutbursts were the accretion disk, the boundary layer, and the accreting WD.

The superoutburst lasted for 15 days, excluding the precursor, and ended on 2021 February 23 (or $\text{JD}^* = 369$) as indicated by the data presented in Figure 2. This superoutburst was followed by an echo outburst, occurring more than a week after the superoutburst ended; these are frequent in SU UMa systems that show only superoutbursts, and have been interpreted by Hameury & Lasota (2021) as the manifestation of an increased mass-transfer rate, possibly as a result of secondary irradiation by the heated accreting WD at the end of a superoutburst. This interpretation is strengthened by the fact that in ASASSN-21au, the system has not returned to full quiescence at the end of the superoutburst.

We now compare the behavior between the X-rays, optical, and UV observations obtained by UVOT. As shown in other AM CVns, during the post-outburst cooling phase of ASASSN-21au there is X-ray emission indicating the presence of residual accretion. Interestingly, during the post-outburst cooling phase the spectrum was substantially redder than during the peak of the superoutburst. A possible explanation for such behavior is that the inner parts of the disk may have evaporated in that cooling phase.

Figure 2 also shows a correlation between the optical, UV, and X-rays. During the optical and UV maxima, the X-ray emission also peaked, and during the optical and UV decay to the post-outburst cooling phase the X-ray flux decreased by a factor of 3. This behavior is different from that observed in the AM CVns KL Dra (Ramsay et al. 2012b) and SDSS J141118+481257 (henceforth SDSS 1411; Rivera Sandoval & Maccarone 2019), where an anticorrelation between the optical/UV and the X-rays during superoutburst was observed. The same anticorrelation has been observed in many CVs (e.g., Wheatley et al. 2003; Byckling et al. 2009; Fertig et al. 2011), where it has been explained as due to changes in the optical depth of the boundary layer.

According to the standard theory (Patterson & Raymond 1985a, 1985b), increases in the X-ray flux with accretion rate are expected so long as the boundary layer remains optically thin; once the boundary layer becomes optically thick, the majority of the flux shifts to the far UV and the X-ray flux drops. Three nearby CVs—SS Cyg, U Gem, and

GW Lib—have shown a clear correlation between X-ray and optical/UV flux. SS Cyg showed this during the early and late parts of its outburst, with an anticorrelation at the highest optical fluxes (and presumably mass-transfer rates; Wheatley et al. 2003). Fertig et al. (2011) summarize observations of six well-studied DN outbursts, in which four showed suppression of the X-rays with increased mass transfer at some point. The peak X-ray luminosities of these CVs (in this paradigm, reflecting the critical accretion rate for the boundary layer to turn optically thick) mostly lie between $L_X = 1 \times 10^{32}$ and 1×10^{33} erg s⁻¹, though VW Hyi showed X-ray suppression from a peak of only 6×10^{30} erg s⁻¹.

However, the critical accretion rate for the boundary layer turning optically thick may be different for He versus H accretion. The peak L_X values for the two AMCVn systems with well-studied outbursts where an anticorrelation has been observed are 5×10^{30} erg s⁻¹ (KL Dra, Ramsay et al. 2012a) using the Gaia distance of 948 pc (Bailer-Jones et al. 2021), and 2×10^{31} erg s⁻¹ (SDSS 1411, Rivera Sandoval & Maccarone 2019). These are substantially smaller than the typical values for H-accreting CVs, suggesting that the critical accretion rate is systematically lower for He accretion. Assuming that ASASSN-21au reaches a peak L_X below the peak L_X of the other two AM CVn systems (to account for its X-ray/optical correlation), its inferred distance should be less than 400 pc. However, since we do not understand the origin of the large scatter in peak L_X values we cannot be too confident of this estimate. It is also possible that the X-ray-emitting region is still optically thin if the accretion disk does not extend to the accreting WD surface, but is, even at large accretion rates, truncated by, e.g., a strong magnetic field.

We do not see clear changes in the X-ray spectral index of ASASSN-21au between the plateau and the post-outburst cooling phase, despite the changes in flux. Photon indices of $\Gamma = 2.2 \pm 0.28$ and $\Gamma = 2.08 \pm 0.56$ were determined for each phase, consistent within the errors.

3.2. ASASSN-21au and the Dichotomy in the Outburst Behavior of AM CVns

3.2.1. Outburst Duration: Disk Instabilities versus Enhanced Mass Transfer

The light curves of ASASSN-21au reveal several interesting characteristics. First, the initial scaled increases in brightness up to day JD* = 349 are slow, of low amplitude, and have a so-called red color evolution (Figure 3 and Section 3.4), reaching ZTF $g - r > 0.5$. Those are the same characteristics observed in the outburst light curves of the AM CVns SDSS J080710+485259 (henceforth SDSS 0807) and SDSS J113732+405458 (henceforth SDSS 1137; Rivera Sandoval et al. 2020, 2021; Sunny Wong et al. 2021), which have P_{orb} close to 53 and 60 minutes, respectively.

Second, on JD* = 349 ASASSN-21au developed a short-duration superoutburst, which contrasts with the outbursts of SDSS 0807 and SDSS 1137, which lasted longer than a year, suggesting that there is more than one mechanism at work in the outbursts of long-period AM CVns. On one hand, a superoutburst lasting for 19 days (including the precursor), with a short rise time, and a plateau phase followed by an abrupt cutoff, as observed in ASASSN-21au, is fully consistent with expectations from the disk instability model (DIM; Cannizzo & Nelemans 2015; Cannizzo & Ramsay 2019). On the other hand, outbursts lasting for more than a year cannot be

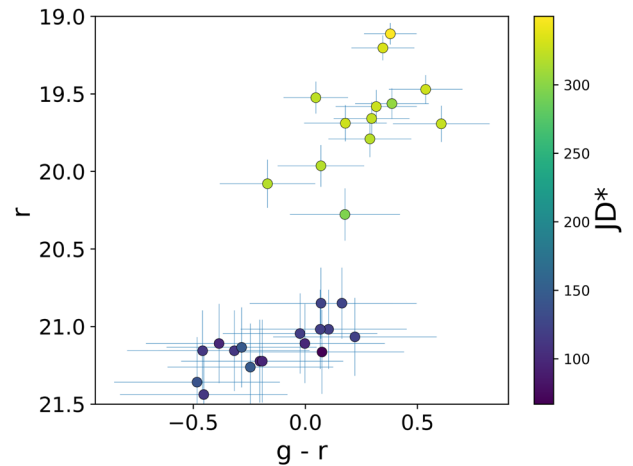


Figure 3. Color evolution for ASASSN-21au during quiescence and the increased levels 1 and 2 as shown in Figure 1 using ZTF data. The binary is redder during the period of increased brightness.

explained by the DIM, for the simple reason that the viscous time (t_{visc} ; Frank et al. 2002) is far too short. The DIM predicts that, during the outburst plateau,¹⁰ the disk is in a quasi-steady state and evolves exponentially on this timescale:

$$t_{\text{visc}} = 6.43 \alpha^{-4/5} \dot{M}_{16}^{-3/10} M_1^{1/4} r_{10}^{11.4} \text{ day}, \quad (1)$$

where $\alpha \sim 0.2$ is the Shakura–Sunyaev parameter in the hot state, \dot{M}_{16} is the mass accretion rate in units of 10^{16} g s⁻¹, M_1 is the primary mass in solar units, and r_{10} is the outer disk radius in units of 10^{10} cm, with $r_{10} \sim 1$ –1.5 for an orbital period close to 1 hr. t_{visc} is much shorter than the observed duration of the whole outburst. An increase in the mass transfer due to irradiation of the secondary does increase the outburst duration, but under the DIM with enhanced mass transfer for the systems with outbursts longer than a year one would need fine tuning to change the outbursts’ duration by almost two orders of magnitude. There are indications from ATLAS data that SDSS 1137’s outburst lasted ~ 650 days.¹¹ If the duration of SDSS 1137’s outburst was in fact longer than previously reported (Rivera Sandoval et al. 2021; Sunny Wong et al. 2021), the difference in duration with ASASSN-21au would be even more remarkable. Another interesting difference among these long-period AM CVn systems is that the U emission in SDSS 1137 seems to have been suppressed, because there was no evidence of an increase in that band (Rivera Sandoval et al. 2021), while in the case of ASASSN-21au there is a clear increase in U during superoutburst (Figure 2).

In Figure 4 we compare the duration of the superoutburst of ASASSN-21au to those of other AM CVns. We have also plotted the duration of the superoutburst of ASASSN-21au when we include the period of increased brightness previous to the superoutburst. This figure shows that there is a clear dichotomy in the outburst duration of long-period AM CVns. Based on the behavior of ASASSN-21au up to day JD* = 349, and the similarities with SDSS 0807 and SDSS 1137, it seems that the mechanism that caused the increases in brightness in

¹⁰ Note that the plateau phase does not mean that there is no evolution, but that the emission evolves much more slowly than during the rise and decline phases.

¹¹ T. Kupfer and J. van Roestel, private communication.

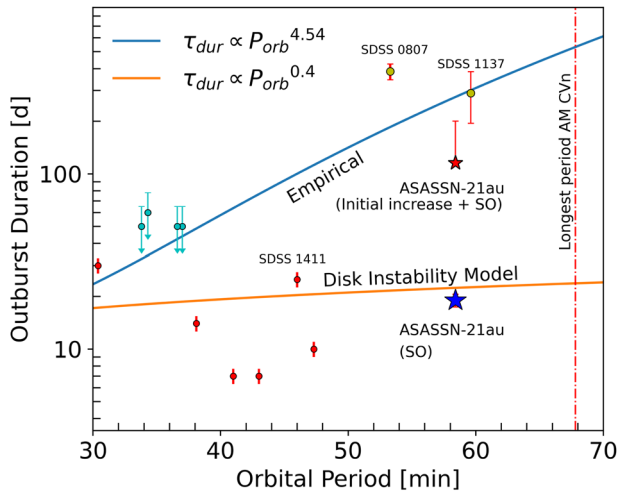


Figure 4. Orbital period (P_{orb}) vs. outburst duration (τ_{dur}) for AM CVns. The duration of the superoutburst (SO) of ASASSN-21au is indicated by a blue star. A red star indicates the duration of the superoutburst including the initial brightenings. The upper error for that red star symbol has been overestimated and it has been determined from the last quiescent ZTF point to the first Gaia detection with increased brightness. The long-period AM CVn SDSS 0807, which had an outburst with a duration longer than a year, is marked in yellow. In the case of SDSS 1137 we have plotted the duration as reported in Rivera Sandoval et al. (2021) but there are indications that the event lasted around 650 days. Red points are other AM CVns as reported by Cannizzo & Ramsay (2019) and references therein. The cyan points are upper limits. The orange line indicates the relation between P_{orb} and τ_{dur} obtained from the DIM by Cannizzo & Ramsay (2019), and the blue line is the empirical relation derived by Levitan et al. (2015). The duration of the SO in ASASSN-21au is consistent with expectations from the DIM, but it is several tens of times shorter than those of SDSS 0807 and SDSS 1137, clearly indicating the existence of a dichotomy. The red dashed line indicates the period of the AM CVn with the longest P_{orb} detected so far (Green et al. 2020). To date, no outbursts have been detected from that binary.

ASASSN-21au favors an enhanced mass-transfer scenario as well. However, the subsequent development of a DIM outburst in ASASSN-21au contrasts with the outburst evolution of SDSS 0807 and SDSS 1137. We stress that inclination effects do not explain such dichotomy given that eclipsing AM CVns (ZTFJ0407-00, YZLMi, PTF1J1919+4815, Gaia14aae) show blue superoutbursts of short duration and large amplitude (e.g., van Roestel et al. 2021b; Duffy et al. 2021; Campbell et al. 2015).

3.2.2. Outburst Decay Times

For the purpose of comparing the decay times, we have fitted the time evolution of the magnitude with a straight line and determined its slope n for ASASSN-21au, SDSS 0807, and SDSS 1137 during the plateau’s decline and post-outburst cooling phase using the ZTF data for consistency (Table 1). However, for the case of ASASSN-21au we also used the AAVSO clear data, which had a better coverage in time for the decay from the plateau ($367 < JD^* < 369$) and early times of the cooling phase ($369 < JD^* < 376.5$, $n = (21.22 \pm 0.84) \times 10^{-3} \text{ mag day}^{-1}$). For this binary we also fitted the decay from the echo outburst ($377.8 < JD^* < 381$) using the ASAS g observations and obtained $n = (1179.80 \pm 46.05) \times 10^{-3} \text{ mag day}^{-1}$. The latter value is consistent with that obtained when fitting the decay part of the superoutburst using the AAVSO data in the clear filter (Table 1). Note that in the case of SDSS 0807 there is substantial scatter in both ZTF bands (r and g) and thus the fit is affected by that. From this analysis one sees that the decay is ~ 3 orders of magnitude steeper in ASASSN-21au than in the other AM CVns systems

during the fast decay from the plateau in both ZTF bands, stressing its different behavior from the other systems.

3.2.3. Mass-transfer Rate and Luminosity Estimates

Since the distance to ASASSN-21au is not known, we are unable to determine the accretion rate to compare it directly to expectations from the DIM. However, rough calculations can be made in order to estimate that parameter. Considering the model by Bildsten et al. (2006) for an AM CVn of period 58 minutes and a massive ($\sim 1 M_{\odot}$) WD, which seems to be appropriate (considering the case of SDSS 1137 with $P_{orb} \sim 60$ minutes and recent estimates of masses in AM CVns; van Roestel et al. 2021b), the absolute V mag of ASASSN-21au should be ~ 13 . As there are no V measurements during quiescence, we instead use the g value from Pan-STARRS ($20.96 \pm 0.06 \text{ mag}$, very similar to Gaia G). This allows us to estimate a distance of 400 pc (consistent with our estimate in Section 3.1, based on peak L_X). By scaling the luminosities to this value one obtains the relations $L_{X, \text{outburst}} = 1.4 \times 10^{31} d_{400}^2 \text{ erg s}^{-1}$ during outburst and $L_{X, \text{post}} = 7.3 \times 10^{30} d_{400}^2 \text{ erg s}^{-1}$ during the early post-outburst cooling phase, where d_{400} is $d/400 \text{ pc}$. On the other hand, the NUV ($UVW2$, $UVM2$, $UVW1$) luminosity is $L_{\text{NUV, outburst}} = 1.6 \times 10^{34} d_{400}^2 \text{ erg s}^{-1}$ and $L_{\text{NUV, post}} = 7.4 \times 10^{31} d_{400}^2 \text{ erg s}^{-1}$, respectively in each state. Assuming that the NUV luminosity during outburst is due to accretion on the WD with $R = 0.008 R_{\odot}$ (similar to Sirius B, and appropriate for a $1 M_{\odot}$ WD), we obtain $\dot{M}_{\text{NUV, outburst}} = 6.7 \times 10^{16} R_{008} d_{400}^2 M_1^{-1} \text{ g s}^{-1}$, where R_{008} is $R/0.008 R_{\odot}$ and M_1 is the mass of the accreting WD in solar masses. The value of \dot{M} would be even larger if we consider the bolometric luminosity. In fact if the extreme UV luminosity is larger than the NUV one (as expected), \dot{M} would be larger than $\dot{M}_{\text{crit}}^+(R_{\text{out}}) = 1.2 \times 10^{17} \text{ g s}^{-1}$ (considering the expressions given in Equation (A.2) of Kotko et al. (2012), and assuming $R_{\text{out}, 10} = 1.3$), as would occur if the full disk is in the hot state. An upper limit on the accretion rate in full quiescence can be determined from the X-ray luminosity during the post-outburst cooling phase.¹² We use the X-ray flux for the upper limit, since in the cooling phase most of the UV flux presumably originates from the hot WD with some contribution from the illuminated inner accretion disk, while the accretion flow is thought to radiate optically thin bremsstrahlung, placing most of the output radiative flux into the X-rays. We find, using the same parameters, that $\dot{M}_{\text{qui}} < 3 \times 10^{13} R_{\text{in}, 008} d_{400}^2 M_1^{-1} \text{ g s}^{-1}$, which is of the same order as $\dot{M}_{\text{crit}}^-(R_{\text{in}})$ if $R_{\text{in}} > d_{400}^{1.2} M_1^{-0.08} \times 10^9 \text{ cm}$, again as expected if the DIM holds.¹³

3.3. The Spectral Energy Distribution of ASASSN-21au in Quiescence

Using archival data obtained during full quiescence we have analyzed the spectral energy distribution, fitting a blackbody to constrain the temperature of ASASSN-21au. We used the GALEX, Pan-STARRS, and Gaia DR3 data, together with a $E(g-r) = 0.05$ (from the 3D dust map of Green et al. 2019) and obtained $T = 14,300 \pm 1600 \text{ K}$, which is roughly consistent with expectations from Bildsten et al. (2006) for an AM CVn of $P_{orb} \sim 58$ minutes and $M \sim 1 M_{\odot}$ WD. It is possible that there is an IR excess because the Pan-STARRS- z data point is 7σ above

¹² In full quiescence the X-ray luminosity must be lower than the observed one during the post-outburst cooling phase.

¹³ Note that, unlike R_{out} , the value of R_{in} is not fixed by the orbital parameters.

Table 1
Slope of the Magnitude Evolution

ID	n of Plateau's Decay (mag day ⁻¹)				n of Cooling Phase (mag day ⁻¹)		
	Dates (JD)	ZTF g ($\times 10^{-3}$)	ZTF r ($\times 10^{-3}$)	Clear ($\times 10^{-3}$)	Dates (JD)	ZTF g ($\times 10^{-3}$)	ZTF r ($\times 10^{-3}$)
ASASSN-21au	2,459,267–2,459,269	1221.83 \pm 9.11	1091.67 \pm 6.67	1141.83 \pm 2.56	2,459,285–2,459,330	8.11 \pm 0.50	8.80 \pm 0.55
SDSS 0807	2,458,591–2,458,816	9.43 \pm 0.18	8.91 \pm 0.17	...	2,458,816–2,459,330	0.83 \pm 0.13	1.24 \pm 0.10
SDSS 1137	2,458,225–2,458,492	1.38 \pm 0.07	2.61 \pm 0.06	...	2,458,568–2,459,330	0.05 \pm 0.02	0.19 \pm 0.02

Note. Values of the slope n when fitting a linear model ($n\tau + b$) to the magnitude evolution during the decay from the plateau and the post-outburst cooling phase of ASASSN-21au, SDSS 0807, and SDSS 1137.

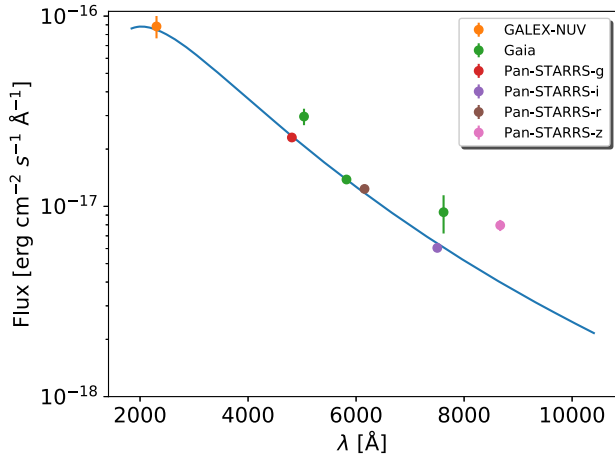


Figure 5. Spectral energy distribution of ASASSN-21au during quiescence using archival data. The blue line denotes the best blackbody fit with a temperature of $14,300 \pm 1600$ K. The z -band point is at 7σ above the fit, possibly due to an excess. Additional IR data are required to confirm this.

the blackbody fit line (Figure 5). However, given that we have only one IR data point, a fit with two blackbodies (accreting WD and disk/donor) is very poorly constrained, leading to practically meaningless results. New, deeper IR observations are needed to confirm this excess. As shown in Bildsten et al. (2006), the contribution of the accretion disk in quiescence should be minimal in the optical, and the hot WD should dominate the optical light in quiescence.

Note that a comparison of the WD temperature based on the spectral energy distribution during the post-outburst cooling phase is not really possible considering the small amount of data obtained in this period. Also, during that phase a contribution from the accretion disk is still expected, which would be difficult to disentangle from the WD emission, especially considering the limited data points available.

3.4. The Varying Color Evolution of ASASSN-21au: The Binary Reveals a Blue Superoutburst

Recently, it has been shown that outbursts in long-period AM CVns have a color evolution that is not compatible with the one expected by the DIM (Rivera Sandoval et al. 2020, 2021). In SDSS 0807 and SDSS 1137 the AM CVns become redder and brighter as they reach the maximum of the outburst. That color evolution together with the duration and amplitude of the outbursts suggests that the outbursts are confined to the outer parts of the disk, perhaps due to enhanced mass transfer from the donor.

In Figure 3 we present the color evolution of ASASSN-21au using the data from ZTF g and r before JD* = 349 (when the

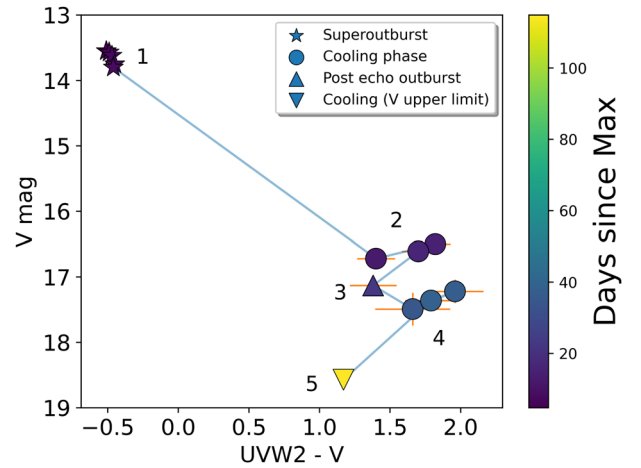


Figure 6. Color evolution for the AM CVn ASASSN-21au with an orbital period of ~ 58 minutes during superoutburst as indicated by the UVOT data in the NUV band $UVW2$ and the optical filter V . The dominant sources of emission are marked with numbers in the plot and are: 1, 3 = disk + WD + boundary layer, 2, 4 = disk, 5 = WD. The point at $UVW2 - V = 1.38$ is bluer than the preceding ones because it was taken at the end of the echo outburst. Afterwards the binary reddens again. The general color evolution of ASASSN-21au is compatible with expectations from the DIM (Hameury et al. 2020). However, the pattern is opposite to the one followed by SDSS 0807 and SDSS 1137 (Rivera Sandoval et al. 2021), indicating that the mechanism that drives the outbursts in these long-period systems is different.

precursor started). We see that the binary becomes slightly redder than in quiescence as it increases its brightness, reaching $ZTF\ g - r > 0.5$. Note that the measurements have large error bars because the binary is faint and is close to the limiting magnitude of ZTF. However, despite the large scatter, one finds that the color behavior of ASASSN-21au is completely compatible with the color evolution observed in SDSS 0807 and SDSS 1137, suggesting then that this part of the light curve in ASASSN-21au can also be explained under an enhanced mass-transfer scenario. Note that during quiescence the binary is blue because the WD is dominating the emission.

On the other hand, in Figure 6 we present the color evolution of ASASSN-21au using the simultaneous UV and optical data obtained by Swift during the superoutburst and post-outburst cooling phase. We chose the bluest ($UVW2$) and reddest (V) UVOT filters to trace the behavior. Figure 6 shows that ASASSN-21au follows an opposite pattern to that observed in SDSS 0807 and SDSS 1137. In the case of ASASSN-21au, the binary becomes bluer and brighter closer to the peak, and as it cools down it becomes redder. Note that in Figure 6 there is a second turn toward bluer colors at a V magnitude of 17.1, which is due to a measurement obtained at the end of the echo outburst, when the accretion disk and accreting WD were still hot. After that, the binary continues becoming redder and

fainter. The last blue turn in that diagram corresponds to the accreting WD becoming the dominant emitting source, and being much brighter in UV than in the optical, where just upper limits were detected in V . A ZTF color evolution of ASASSN-21au during outburst in g and r is also displayed in Figure 7 of the Appendix.

The color evolution of ASASSN-21au during superoutburst is similar to that of the binary systems SDSS 1411 (Rivera Sandoval et al. 2021), PTF 0719+4858, and SDSS J1043+5632 (Pichardo Marcano et al. 2021). It is also compatible with expectations from the DIM (Hameury et al. 2020). This strengthens our conclusion that the main mechanism responsible for the superoutbursts (after $\text{JD}^* = 349$) in ASASSN-21au is a disk instability.

4. Discussion

From the theoretical point of view, two parameters that play a very important role in the DIM are the mass-transfer rate and the truncation radius of the inner disk. The disk is unstable if the mass-transfer rate \dot{M} is in the range $\dot{M}_{\text{crit}}^-(R_{\text{in}}) < \dot{M} < \dot{M}_{\text{crit}}^+(R_{\text{out}})$ where \dot{M}_{crit}^- and \dot{M}_{crit}^+ are the critical mass-transfer rates for being on the cold and hot branches, estimated at the inner and outer disk radii, respectively. In the case of CVs, the actual mass-transfer rate is observed to vary significantly between systems at a given orbital period, meaning that the actual mass-transfer rate deviates from its secular mean, which, in principle, depends mainly on the orbital parameters (e.g., Knigge et al. 2011; Dubus et al. 2018). It is then not difficult to believe that something similar occurs in some AM CVns.

Furthermore, disk truncation in CVs has also been demonstrated to exist. For example, observational estimates of the inner disk radius during quiescence have been reported to be larger than the WD radius (Balman & Revnivtsev 2012). Disk truncation occurs if the WD's magnetic field is strong enough to alter the accretion flow, or if the accretion flow becomes optically thin and geometrically thick close to the WD. There are no strong observational constraints on this, but there is a mere indication that the latter mechanism might be preferred in some systems (see, e.g., Hameury & Lasota 2021). Disk truncation is important for cold and stable accretion disks in X-ray binaries and CVs (e.g., Dubus et al. 2018). But in AM CVns that is not a necessary condition for the binary to have a cold and stable disk, because extremely small mass-transfer rates are expected to be present in long-period AM CVns due to their evolution (e.g., Bildsten et al. 2006; Deloye et al. 2007), which would be sufficient to meet the condition $\dot{M}_{\text{crit}}^-(R_{\text{in}}) > \dot{M}$ and so to have cold and stable disks (e.g., Kotko et al. 2012). It is also important to point out that these extremely low mass-transfer rates in AM CVns could make the accretion disks somehow different from those in CVs. For example, the optically thick assumption might not be valid. Furthermore, an additional parameter to the previously mentioned ones could be at play in AM CVns: the metallicity, which ultimately translates to the kind of donor, and which would affect the optical thickness of the disk as well.

The characteristics of the light curve of ASASSN-21au, its similarities and differences to the light curves of SDSS 0807 and SDSS 1137, are then compatible with the following scenario: enhanced mass transfer could be the mechanism that triggers the increases in brightness in the three AM CVns, thus explaining their low amplitude, slow increase in brightness, and red color evolution. The red color is in agreement with the

outer parts of the disks being the dominant sources of emission, perhaps due to a larger contribution from the hot spot.

It is important to note that the long outbursts observed in SDSS 0807 and SDSS 1137 appear to be rather unusual in the zoo of compact binaries. (i) Even if reports of long-term increases before a DIM outburst have been reported in other binaries, they are quite different. For example, CVs of the type Z Cam can show long standstills between (short) normal outbursts due to an increase in the accretion rate, but the behavior and timescales (e.g., much faster rise and decay) of a Z Cam star are different to what is observed in SDSS 1137 and SDSS 0807 (see, e.g., Oppenheimer et al. 1998, for a long-term light curve of Z Cam). Low-mass X-ray binaries have also shown standstills lasting years between outbursts. However, such a mechanism is also analogous to that of Z Cam stars (e.g., Swift J1753.5-0127, Shaw et al. 2019). (ii) SDSS 1137 and SDSS 0807 show clearly distinguishable outbursts instead of erratic transitions between high and low states as observed in other CVs. These include systems with high mass-transfer rates, such as VY Scl and some intermediate polars such as FO Aqr (see, e.g., Kennedy et al. 2020) and AM Her (which shows low states). These contrasts, however, should not come as a surprise, given the large difference in the secondaries of AM CVns and CVs. It is then clear that the outbursts in the long-period AM CVns SDSS 1137 and SDSS 0807 do not have an origin in disk instabilities and so far have no counterpart in CVs or X-ray binaries.

If there are mass enhancements for ASASSN-21au, they could even occur at different rates, considering the two different brightness levels observed prior to the superoutburst. At a later stage, mass enhancement could have produced disk instabilities in ASASSN-21au, either due to a further increase in the mass-transfer rate or to the accretion disk accumulating enough mass at the same increased mass-transfer rate before the superoutburst. This would explain the fast, large-amplitude blue superoutburst observed in ASASSN-21au, which is consistent with expectations from the DIM. The presence of mass enhancement would also explain the increased magnitude after the superoutburst in ASASSN-21au and the presence of an echo outburst at later times (see Section 3.1). The observations of ASASSN-21au during superoutburst clearly contrast to what has been observed in other AM CVn systems with similar long orbital periods, thus revealing a dichotomy in their behavior.

It is unclear why instabilities were not observed in SDSS 0807¹⁴ and SDSS 1137, but under an enhanced mass-transfer scenario, the mass-transfer rate could have been low enough such that the condition $\dot{M}_{\text{crit}}^-(r_{\text{in}}) > \dot{M}$ was never violated. As mentioned before, increases in brightness have been observed to exist previous to DIM outbursts in other accreting WDs (e.g., SS Cyg) and X-ray binaries (e.g., Bernardini et al. 2016; Goodwin et al. 2020; Kimura et al. 2021). However, we point out that one should be cautious when comparing such phenomena to the event presented in this paper given the difference in mass-transfer rates as well as in the secondary's structure and composition. For example, SS Cyg has a mass-transfer rate in quiescence that is ~ 4 orders of magnitude larger (Miller-Jones et al. 2013) than that expected for ASASSN-21au, SDSS 0807, or SDSS 1137,

¹⁴ Given the slightly blue color evolution of SDSS 0807 near the peak of the outburst, Rivera Sandoval et al. (2021) discussed the possibility that disk instabilities could have developed during that phase. However, although that scenario cannot be discarded, it is not very likely considering the observed values of $g - r$ in that phase and the timescales expected from the DIM as discussed in this paper, which were not observed in the case of SDSS 0807.

which for CVs places SS Cyg well within the expected unstable regime of the DIM, producing then consistent results with that model. On the other hand, AM CVn systems with long orbital periods must have a mass-transfer rate higher than the secular mean for a disk instability to be triggered, and, as discussed previously, when the mass-transfer rate is extremely low, it can lead to different disk behavior.

5. Conclusion

In this paper we have shown observational evidence that a dichotomy exists in the outburst properties of long-period AM CVns. Short outbursts are most likely caused by a disk instability, whereas outbursts lasting for a year or more cannot be explained by the DIM and are probably due to a long-lasting mass-transfer event. The whole behavior of ASASSN-21au is consistent with a scenario in which initial mass enhancement produced disk instabilities at later times, contrary to what has been observed in other long-period AM CVns. Additional studies of similar systems are needed to fully confirm this scenario. At present, the origin and characteristics of mass-transfer events remain a mystery; they have also been postulated in systems such as CVs close to the minimum period that exhibit rare superoutbursts (the WZ Sge systems). The causes of such phenomena need to be further investigated through high-quality and multiwavelength observations of AM CVns both during outbursts and in quiescence.

We thank the referee for her/his comments which improved the manuscript. C.H. is supported by NSERC Discovery Grant RGPIN-2016-04602. L.E.R.S. was supported by an Avadh Bhatia Fellowship at the University of Alberta and a Gruber-IAU Fellowship during the realization of this work. The authors acknowledge the Swift team for scheduling the target-of-opportunity requests. The authors also acknowledge the ATLAS, ASAS-SN, Pan-STARRS, and VizieR databases for providing part of the data presented in this paper. This work has made use of data from the European Space Agency (ESA) mission Gaia (<https://www.cosmos.esa.int/gaia>), processed by the Gaia Data Processing and Analysis Consortium (DPAC, <https://www.cosmos.esa.int/web/gaia/dpac/consortium>). Funding for the DPAC has been provided by national institutions, in particular the institutions participating in the Gaia Multilateral Agreement. We acknowledge the Photometric Science Alerts Team (<http://gsaweb.ast.cam.ac.uk/alerts>). Based on observations obtained with the Samuel Oschin 48 inch Telescope at the Palomar Observatory as part of the Zwicky Transient Facility project. ZTF is supported by the National Science Foundation under grant No. AST-1440341 and a collaboration including Caltech, IPAC, the Weizmann Institute for Science, the Oskar Klein Center at Stockholm University, the University of Maryland, the University of Washington, Deutsches Elektronen-Synchrotron and Humboldt University, Los Alamos National Laboratories, the TANGO Consortium of Taiwan, the University of Wisconsin at Milwaukee, and Lawrence Berkeley National Laboratories. Operations are conducted by COO, IPAC, and UW.

Appendix

The Color Evolution of ASASSN-21au during Superoutburst

Figure 7 shows the color evolution of ASASSN-21au using the ZTF data.

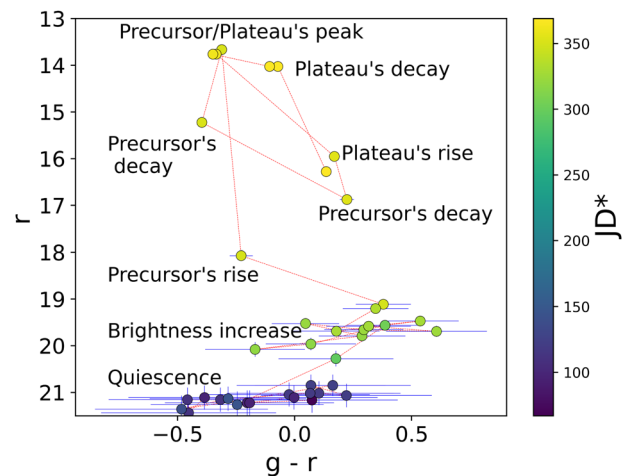


Figure 7. Color evolution based on ZTF data of ASASSN-21au with an orbital period ~ 58 minutes up to the end of the plateau phase of the superoutburst. The binary is initially blue due to the WD dominating the emission during quiescence. During the increased brightness levels 1 and 2 (see Section 3.1) the binary increases in brightness and becomes redder. When the precursor of the superoutburst starts, ASASSN-21au becomes blue. The same behavior is observed when the rise of the plateau occurs. The binary becomes redder during the decay of the precursor and the decay of the plateau.

ORCID iDs

L. E. Rivera Sandoval <https://orcid.org/0000-0002-9396-7215>
 C. O. Heinke <https://orcid.org/0000-0003-3944-6109>
 J. M. Hameury <https://orcid.org/0000-0002-6412-0103>
 Y. Cavecchi <https://orcid.org/0000-0002-6447-3603>
 T. Vanmunster <https://orcid.org/0000-0002-8116-6429>
 F. D. Romanov <https://orcid.org/0000-0002-5268-7735>

References

- Arnaud, K. A. 1996, ASP Conf. Ser. 101, *Astronomical Data Analysis Software and Systems V*, ed. G. H. Jacoby & J. Barnes, (San Francisco, CA: ASP), 17
- Bailer-Jones, C. A. L., Rybizki, J., Fouesneau, M., Demleitner, M., & Andrae, R. 2021, *AJ*, 161, 147
- Balman, S., & Revnivtsev, M. 2012, *A&A*, 546, A112
- Bernardini, F., Russell, D. M., Shaw, A. W., et al. 2016, *ApJL*, 818, L5
- Bianchi, L., Herald, J., Efremova, B., et al. 2011, *Ap&SS*, 335, 161
- Bildsten, L., Townsley, D. M., Deloye, C. J., & Nelemans, G. 2006, *ApJ*, 640, 466
- Breivik, K., Kremer, K., Bueno, M., et al. 2018, *ApJL*, 854, L1
- Byckling, K., Osborne, J. P., Wheatley, P. J., et al. 2009, *MNRAS*, 399, 1576
- Campbell, H. C., Marsh, T. R., Fraser, M., et al. 2015, *MNRAS*, 452, 1060
- Cannizzo, J. K., & Nelemans, G. 2015, *ApJ*, 803, 19
- Cannizzo, J. K., & Ramsay, G. 2019, *AJ*, 157, 130
- Cash, W. 1979, *ApJ*, 228, 939
- Chambers, K. C., Magnier, E. A., Metcalfe, N., et al. 2016, arXiv:1612.05560
- Deloye, C. J., Taam, R. E., Winisdoerffer, C., & Chabrier, G. 2007, *MNRAS*, 381, 525
- Drake, A. J., Djorgovski, S. G., Mahabal, A., et al. 2009, *ApJ*, 696, 870
- Dubus, G., Otulakowska-Hypka, M., & Lasota, J.-P. 2018, *A&A*, 617, A26
- Duffy, C., Ramsay, G., Steeghs, D., et al. 2021, *MNRAS*, 502, 4953
- Fertig, D., Mukai, K., Nelson, T., & Cannizzo, J. K. 2011, *PASP*, 123, 1054
- Frank, J., King, A., & Raine, D. J. 2002, *Accretion Power in Astrophysics* (3rd ed.; Cambridge: Cambridge Univ. Press)
- Gaia Collaboration 2020, yCat/350
- Goodwin, A. J., Russell, D. M., Galloway, D. K., et al. 2020, *MNRAS*, 498, 3429
- Green, G. M., Schlafly, E., Zucker, C., Speagle, J. S., & Finkbeiner, D. 2019, *ApJ*, 887, 93
- Green, M. J., Marsh, T. R., Carter, P. J., et al. 2020, *MNRAS*, 496, 1243
- Grindlay, J., Tang, S., Simcoe, R., et al. 2009, ASP Conf. Ser. 410, *Preserving Astronomy's Photographic Legacy: Current State and the Future of North*

- American Astronomical Plates, ed. W. Osborn & L. Robbins, (San Francisco, CA: ASP), 101
- Hameury, J. M. 2020, *AdSpR*, **66**, 1004
- Hameury, J. M., Knigge, C., Lasota, J. P., Hamsch, F. J., & James, R. 2020, *A&A*, **636**, A1
- Hameury, J. M., & Lasota, J. P. 2021, *A&A*, **650**, A114
- Iben, I. J., & Tutukov, A. V. 1991, *ApJ*, **370**, 615
- Isogai, K., Tampo, Y., Kojiguchi, N., et al. 2021, *ATel*, **14390**, 1
- Kafka, S. 2021, Observations from the AAVSO International Database, <https://www.aavso.org>
- Kennedy, M. R., Garnavich, P. M., Littlefield, C., et al. 2020, *MNRAS*, **495**, 4445
- Kimura, M., Yamada, S., Nakaniwa, N., et al. 2021, *PASJ*, **73**, 1262
- Knigge, C., Baraffe, I., & Patterson, J. 2011, *ApJS*, **194**, 28
- Kochanek, C. S., Shappee, B. J., Stanek, K. Z., et al. 2017, *PASP*, **129**, 104502
- Kotko, I., Lasota, J. P., Dubus, G., & Hameury, J. M. 2012, *A&A*, **544**, A13
- Levitan, D., Groot, P. J., Prince, T. A., et al. 2015, *MNRAS*, **446**, 391
- Levitan, D., Kupfer, T., Groot, P. J., et al. 2013, *MNRAS*, **430**, 996
- Liu, W.-M., Jiang, L., & Chen, W.-C. 2021, *ApJ*, **910**, 22
- Lomb, N. R. 1976, *Ap&SS*, **39**, 447
- Masci, F. J., Laher, R. R., Rusholme, B., et al. 2019, *PASP*, **131**, 018003
- Miller-Jones, J. C. A., Sivakoff, G. R., Knigge, C., et al. 2013, *Sci*, **340**, 950
- Nelemans, G., Yungelson, L. R., van der Sluys, M. V., & Tout, C. A. 2010, *MNRAS*, **401**, 1347
- Nelson, L. A., Rappaport, S. A., & Joss, P. C. 1986, *ApJ*, **311**, 226
- Oppenheimer, B. D., Kenyon, S. J., & Mattei, J. A. 1998, *AJ*, **115**, 1175
- Patterson, J., Kemp, J., Harvey, D. A., et al. 2005, *PASP*, **117**, 1204
- Patterson, J., & Raymond, J. C. 1985a, *ApJ*, **292**, 535
- Patterson, J., & Raymond, J. C. 1985b, *ApJ*, **292**, 550
- Pichardo Marcano, M., Rivera Sandoval, L. E., Maccarone, T. J., & Scaringi, S. 2021, *MNRAS*, **508**, 3275
- Pringle, J. E., & Webbink, R. F. 1975, *MNRAS*, **172**, 493
- Ramsay, G., Barclay, T., Steeghs, D., et al. 2012a, *MNRAS*, **419**, 2836
- Ramsay, G., Green, M. J., Marsh, T. R., et al. 2018, *A&A*, **620**, A141
- Ramsay, G., Wheatley, P. J., Rosen, S., Barclay, T., & Steeghs, D. 2012b, *MNRAS*, **425**, 1486
- Rivera Sandoval, L. E., & Maccarone, T. J. 2019, *MNRAS*, **483**, L6
- Rivera Sandoval, L. E., Maccarone, T. J., Cavecchi, Y., Britt, C., & Zurek, D. 2021, *MNRAS*, **505**, 215
- Rivera Sandoval, L. E., Maccarone, T. J., & Pichardo Marcano, M. 2020, *ApJL*, **900**, L37
- Savonije, G. J., de Kool, M., & van den Heuvel, E. P. J. 1986, *A&A*, **155**, 51
- Scargle, J. D. 1982, *ApJ*, **263**, 835
- Shappee, B. J., Prieto, J. L., Grupe, D., et al. 2014, *ApJ*, **788**, 48
- Shaw, A. W., Tetarenko, B. E., Dubus, G., et al. 2019, *MNRAS*, **482**, 1840
- Sunny Wong, T. L., van Roestel, J., Kupfer, T., & Bildsten, L. 2021, *RNAAS*, **5**, 3
- Tonry, J. L., Denneau, L., Heinze, A. N., et al. 2018, *PASP*, **130**, 064505
- Tutukov, A. V., Fedorova, A. V., Ergma, E. V., & Yungelson, L. R. 1985, *SvAL*, **11**, 52
- Tutukov, A. V., & Yungelson, L. R. 1979, *AcA*, **29**, 665
- van Roestel, J., Creter, L., Kupfer, T., et al. 2021a, *AJ*, **162**, 113
- van Roestel, J., Kupfer, T., Green, M. J., et al. 2021b, *MNRAS*
- Wheatley, P. J., Mauche, C. W., & Mattei, J. A. 2003, *MNRAS*, **345**, 49
- Yungelson, L. R. 2008, *AstL*, **34**, 620